ISSN 1070-3632, Russian Journal of General Chemistry, 2010, Vol. 80, No. 3, pp. 555–566. © Pleiades Publishing, Ltd., 2010.
Original Russian Text © R.A. Andrievskii, A.V. Khachoyan, 2010, published in Rossiiskii Khimicheskii Zhurnal, 2010, Vol. 53, No. 2, pp. 4–14.

Role of Size-Dependent Effects and Interfaces in Physicochemical Properties of Consolidated Nanomaterials

R. A. Andrievskii[a] and A. V. Khachoyan[b]

[a] *Institute of Chemical Physics Problems, Russian Academy of Sciences, prosp. Akad. Semenova 1, Chernogolovka, Moscow Oblast, 142432 Russia*
e-mail: ara@icp.ac.ru

[b] *Institute of Structural Macrokinetics and Materials Science Problems, Russian Academy of Sciences, prosp. Akad. Semenova 1, Chernogolovka, Moscow Oblast, 142432 Russia*
e-mail: khatch@ism.ac.ru

Received January 10, 2009

Abstract—The major distinctive features of size-dependent effects in nanomaterials were specified. The surface energy, melting temperature, phase equilibria, phonon spectrum, electronic structure, and conductivity type were analyzed in relation to the crystallite size for consolidated nanomaterials based on metals, alloys, intermetallics, carbides, borides, nitrides, oxides, and semiconductors. The interface effects in physicochemical properties of nanomaterials were highlighted. Special attention was given to little studied issues.

DOI: 10.1134/S1070363210030370

INTRODUCTION

Size-dependent effects (i.e., the influence of the characteristic size of grains, particles, phase inclusions, and pores on the properties of materials and substances) fall within the scope of modern nanomaterials science in regard to virtually all types of nanomaterials [1–22]. These effects are of special importance for consolidated nanomaterials, i.e., those comprised of consolidated, rather than isolated or loosely bound nanograins (nanocrystallites). Such compacts (consolidated bulk nanomaterials), films, and coatings are prepared by powder and film technologies, intense plastic deformation, controlled crystallization from the amorphous state, and other techniques. Size-dependent effects in these nanomaterials are manifested as follows [13]:

– interfaces become of increasing importance with crystallite size reduction [it can easily be shown that the interface proportion in the overall structure can be expressed as $\sim 6b/L$, where $2b$ is the boundary (near-boundary area) width which is typically taken as ~1 nm; hence, at the crystallite size decreasing from 10^3 to 10^2 (the conditional upper limit of the grain size L for nanomaterials) and further to 10 nm, the proportion of interfaces will significantly increase from 0.3 to 3 and 30%, respectively];

– the interface properties at the nanometer scale differ from those of coarse-crystalline objects (in the case of nanomaterials, there is an increasing number of triple junctions, along with ordinary grain boundaries, and inorganic–organic hybrid nanomaterials are characterized by diversified interfaces);

– crystallites, particles, etc. can decrease in size to a level comparable to some characteristic physical lengths (e.g., the mean free path of carriers in transport phenomena);

– there can be quantum size effects in nanomaterials, e.g., when the grain (or free carrier localization area) size is comparable with de Broglie wavelength; in metallic nanomaterials these effects can have implications for properties associated with, e.g., conductivity, only for crystallites measuring less than ~1 nm in size; for semiconductors, in particular, narrow-band compounds like InSb and semimetals (Bi), the de Broglie wavelength is much larger, ca. 100 nm; and

– because of specific technologies and nonequilibrium nature of nanomaterials size-dependent effects in them are often masked by other factors (residual stress, boundary segregations, nonequilibrium phases, crystallite size distribution, texture, boundary

condition, etc.), which complicates identification of the "pure" role played by size-dependent effects in nanomaterials as against coarse-crystalline materials.

The above-mentioned features can affect the property–grain size dependences. In many cases, studies of the properties of nanomaterials in relation to the crystallite size revealed special, e.g., inflection, points in these dependences. Many factors can contribute thereto (a change to a different size-dependent mechanism, progressive accumulation of intercrystallite segregations, etc.) which cannot be always predicted.

Here, we analyzed and summarized the latest data on the thermodynamic characteristics, in particular, phase equilibria, as well as on conducting properties of diversified nanofilms, nanotubes, nanowires, and bulk nanocompacts (metals, alloys, intermetallics, high-melting compounds, selected semiconductors). This choice was dictated by our scientific interests driven by the desire to continue exploration of, above all, consolidated nanomaterials. At the same time, mechanical, catalytic, and biological properties of nanomaterials, as well as the cluster and polymer aspects, deserve special detailed consideration; they are beyond the scope of this study. However, in certain cases we attracted these data, in particular, for discussing the surface energy of nanomaterials.

Surface Energy

Apart from being of fundamental importance, surface energy is also essential for numerous materials science and engineering applications (calculation of phase diagrams, assessment of fracture, milling, dilution, wetting, nucleation, coagulation, and coalescence in self-organization of structures, etc.). This makes of special importance the identification of changes in surface energy, associated with particle size reduction to nanoscale. Since Tolman established in 1949 the size dependence of the surface energy, various chemical and physical approaches (in many cases this is certainly a conditional differentiation) were many a time employed to theoretically analyze this issue (see, e.g., [8, 9, 16, 19, 23–28, 31, 32]).

We will omit the calculational details and report the results in general.

Rusanov [18] established the following relationship between the surface energy σ and the surface curvature radius r of a nanoparticle

$$\sigma(r) = -\pi\rho^2\omega/24\,[1 - \ln(2r)/r^2 - 1/16r^4], \quad (1)$$

where ρ is density, and ω, London's constant.

Expression (1) suggests a monotonic increase in surface energy with increasing nanoparticle size. The correction $g(r)$ to the ordinary σ value, reduced to the capillary pressure, can be represented as

$$g(r) = [2\ln(2r) - 1 + 1/4r^2]/[2r^2 - 2\ln(2r) - 1/8r^2]. \quad (2)$$

This correction, very small for large particles, becomes appreciable (~10%) at $r < 5$ nm only.

Samsonov et al. [23, 24] approximated the size dependence of the surface energy (surface tension) of nanocrystals and nanodrops by two formulas

$$\sigma(r) = Kr \text{ at } r < r_0;\ \ \sigma(r) = \sigma_0 \text{ at } r > r_0, \quad (3)$$

where r_0 is the critical radius of 2–10 nm, and K, proportionality coefficient.

The former of these two formulas coincides with that proposed by Rusanov as early as 1960s.

Weissmüller [8, 9] described the surface energy of an isolated spherical nanocrystal with diameter $2r$ as:

$$\sigma(r) = \sigma_0(1 - t/r), \quad (4)$$

where t is the thickness of the subsurface layer in which the excess free energy is localized. It was shown that, at reasonable values $t \approx 0.35$ nm and $2r = 5$ nm, the decrease in σ_0 can be estimated at ~14%, which nearly coincides with the value obtained by formula (1).

Magomedov [25, 26] established relationships between the surface energy and the size and shape of n-dimensional nanocrystals, taking into account relevant shapes and temperatures. For example, for face-centered crystal structures (e.g., silver) with 10^3 atoms ($r_{Ag} \approx 1.5$ nm) σ decreases by ~4 %; in changing to noncubic nanocrystals the $\sigma_0 - \sigma_r$ difference slightly increases.

Decreases in surface energy with decreasing nanocrystal size were also observed in, e.g., [27, 28]. For example, the calculated $\sigma = f(r)$ dependences for silver and lead sulfide nanoparticles suggest a decrease in σ starting from diameter D close to 15 and 10 nm, respectively. Nanda et al. [31, 32] examined evaporation of Ag and PbS nanoparticles (D = 7–40 nm). Processing of the experimental data by the Thomson (Kelvin) formula (relating the saturated vapor pressure above the drop surface to its radius) yielded results exceeding the reference data ($\sigma_{Ag} \approx 1.15$ J m^{-2}; σ_{PbS} = 1–1.4 J m^{-2}). On this basis, the tendency to increase rather than decrease with decreasing nanoparticle radius was inferred for the surface energy (see also

[29, 30]). However, those results differ from the σ values (average) measured electrochemically for Ag nanoparticles, ~0.2 J m^{-2} (r = 50 nm) and ~0.7 J m^{-2} (r = 150 nm) [33]. Most likely, data by Nanda et al. [31, 32] should be qualified as biased.

It should be noted that experimental study of the size-dependent effects as applied to surface properties of nanoobjects is a fairly complex task. This is associated with the difficulties in preparation of the initial samples and their possible changes during measurements. Many researchers (see, e.g., [27]) believe that the results reported in [31, 32] were affected by ambient conditions. This seems especially likely in view of the fact that, in those experiments, the nanoparticle size strongly exceeded the critical value r_o below which a decrease in surface energy is "sensed" [8, 9, 16, 18, 23, 24, 27].

So far, we discussed the results pertinent mainly to isolated nanoparticles. As to surface energy at grain boundaries in nanomaterials, the publications by Andrievskii et al. [1, 13] still remain virtually unique among relevant studies. Weissmüller [8] suggested that, as applied to consolidated nanomaterials, relationship (4) should be transformed into:

$$\sigma(r) = \sigma_0[1 + t/(r - t)]. \quad (5)$$

This expression implies a different size-dependent pattern for the surface energy. The situation is further complicated by the need to consider the progressive influence of triple junctions and diminishing role of grain boundaries in the nanostructure at grain sizes under ~6 nm [13]. Simulations of nanostructured metals with due regard to the contribution from triple junctions showed the following. Nanograin size reduction causes a decrease in the excess boundary enthalpy, i.e., in the boundary surface energy [34]. This was qualitatively supported by the experimental data for 8–23-nm selenium particles (similar results were earlier obtained for $Ni_{80}P_{20}$ nanoalloys [35]).

Ouyang et al. [36] calculated the interfacial surface energy of Ag–Ni nanofilms as comprised of the chemical component (characterizing the bonding energy for Ag–Ni interface) and the elastic component (associated with distinctions in the elastic properties and mismatches of the lattice periods and orientations). That study revealed a decrease in the chemical component with film thinning, in parallel with an increase in the elastic component, which, on the whole, led to a decrease in the total interfacial energy. A decrease in film thickness from ~1 to 0.4 nm caused σ to decrease from 0.9 to ~0.7 J m^{-2}.

Size-dependent effects in surface processes can be exemplified by wetting. As known, the degree of wetting is characterized by the contact angle θ described by following relationship (Young's law):

$$\cos\theta = (\sigma_{sg} - \sigma_{sl})/\sigma_{lg},$$

where σ_{sg}, σ_{sl}, and σ_{lg} are the surface energy at the solid–gas interface, surface energy at the solid–liquid interface, and surface tension of the liquid at the liquid–gas interface, respectively.

In the case of nanodrops the equilibrium between the surface energy components will be described by this equation added with the following term:

$$\cos\theta^* = \cos\theta - k/\sigma_o r, \quad (6)$$

where k is the linear tension (10^{-7}–10^{-6} mN) [37].

It can easily be seen that this term becomes significant at nanodrop radii r under ~10 nm. The surface roughness at the nanohillock level also affects the equilibrium contact angle [21].

Penetration or formation of liquid interlayers at grain boundaries (interfaces) implies

$$\sigma_{ij} \geq 2\sigma_{il}\cos\psi/2, \quad (7)$$

where σ_{ij} is the surface energy for adjoining grains ($i = j$) or phases ($i \neq j$); σ_{il}, surface energy at the solid–liquid interface; and ψ, dihedral angle.

To our knowledge, the applicability of this relationship to nanosystems as adjusted for possible size-dependent effects still remains to be analyzed.

Melting Temperature. Phase Transformations. Phase Diagrams

Melting temperature of nanoparticles and thin films tends to significantly decrease with increasing amplitude of atomic vibrations in surface layers. A number of theoretical expressions were suggested for describing size-dependent effects in terms of melting characteristics (see, e.g., [13, 14, 17, 19–21, 37–42]), in particular

$$T_m(r)/T_m \sim 1 - B/r, \quad (8)$$

$$T_m(h)/T_m \sim 1 - 2(\sigma_{sg} - \sigma_{lg})/H_m h, \quad (9)$$

where T_m, H_m are the melting temperature and enthalpy of melting, respectively; $T_m(r)$ and $T_m(h)$, melting temperatures of the particle with radius r and film with thickness h, respectively; and B, a constant dependent on the density, surface energy, and melting enthalpy of the object.

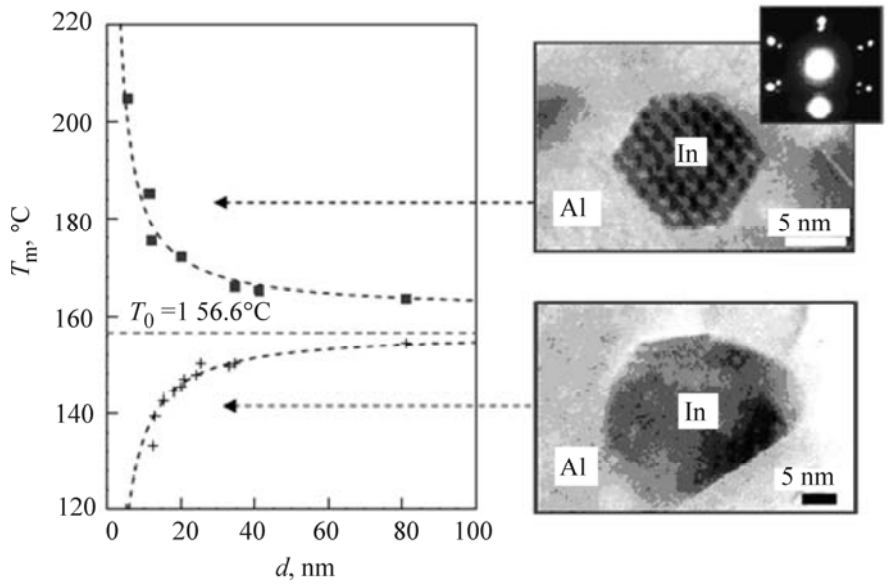

Fig. 1. Melting temperature of In–Al (matrix) nanoobjects vs. indium nanoparticle diameter for (■) coherent and (*x*) incoherent interfaces [46]. The right picture represents the electron images of the In particles.

Virtually all the considered formulas predict that the melting temperature will be proportional to reciprocal particle radius or film thickness, $1/r(h)$. The latest calculations applied corrections to allow for the influence of shape of the particles and the distance separating them from the substrate [41], as well as from the fractal structure [42], amorphous state [40], etc. In particular, it was shown that the $T_m = f(r)$ dependences can exhibit nonmonotonic patterns [38, 40] (further researches are needed to reveal the responsible physical factors and provide experimental validation).

Using simple geometrical approaches and a general expression $T_m(r) = T_m(1 - N/2n)$, where N and n are the number of surface atoms and the total number of atoms in nanoobject, respectively, Qi [43] elucidated the trends in T_m for a spherical nanoparticle, nanowire, and nanofilm with identical intrinsic dimensions. The above-given expression is based on the proportionality between the melting temperature and cohesion energy, with the latter comprised of the bulk and surface components. The N/n parameters for a spherical particle, a wire, and a film can be represented as $4d/D$, $8d/3l$, and $4d/3h$, respectively, where d is the atomic diameter; D, particle diameter; l, wire diameter; and h, film thickness. Hence, at $D = l = h$ the largest decrease in T_m will be observed for nanoparticles, and a slightly smaller, for nanowires and nanofilms prepared from the same material. Experimental data for indium nanowires and nanofilms basically support the results derived from analysis with this simple procedure.

For nanoparticles (nanowires and nanoplates) incorporated into a matrix prepared from a different material, a decrease in intrinsic dimension can cause not only decrease but also increase in the melting temperature (superheating). Whether the melting temperature of a matrix nanoobject will decrease of increase will depend on the specific condition of the interfaces (i.e., on the degree of disordering and stress condition at interfaces in nanocomposites) and on the difference in thermal expansion coefficients, elastic characteristics, and densities between solid and liquid states. Certain role can also be played by capillary effects.

Increase in T_m was observed for Ag–Ni (matrix) [44], Ge–SiO_2 (matrix) [45], and Pb (In)–Al (matrix) [46, 47] nanoobjects. Of special interest are the data for In–Al (matrix) nanoobjects for which T_m can both decrease (for objects prepared by intense grinding), and increase (for annealed objects or those prepared by spinning, i.e., quenching from the liquid state) (Fig. 1). The melting behavior of these components is clearly dominated by the inclusion particle morphology. Relevant electron-microscopic examinations for nanoparticles prepared by the grinding technique revealed the lack of faceting on the surface (incoherent

Table 1. Nanomaterials with unusual phase compositions [51]. Crystal lattice structure designations: (hcp) hexagonal close-packed; (fcc) face-centered cubic; (bcc) body-centered cubic; (M) monoclinic; (T) tetragonal; and (C) cubic

Object	Lattice type		Reference
	normal phase composition (standard conditions)	phase composition of nanomaterials	
Co	hcp (α-Co)	fcc (β-Co)	[52]
Ti	hcp (α-Ti)	bcc (β-Ti)	[53]
Fe-Ni	Martensite	fcc (austenite)	[54]
ZrO_2	M	T	[21, 55–58]
TiO_2	Rutile	Anatase	[59]
Al_2O_3	α-Al_2O_3	γ-Al_2O_3	[60]
Y_2O_3	C (α-Y_2O_3)	M (γ-Y_2O_3)	[61]
CdSe, CdS	Wurtzite	NaCl	[62]
$BaTiO_3$	C	T	[21, 59]
$PbTiO_3$	C	T	[59]

interfaces), along with the ensuing high interfacial surface energies and T_m decreasing with decreasing particle size. The faceting, i.e., coherent interfaces, is appreciable for objects prepared by spinning (or annealed, as in the case of Pb–Al nanoobjects [46]); it leads to a decrease in the interfacial energy and an increase in T_m with decreasing nanoparticle size.

Qi [48] suggested describing T_m of nanowires and nanoplates in matrices as:

$$T_m(l, h)/T_m = 1 - 3c(2 - p - pq)/8, \qquad (10)$$

where $c = N/n$; p is interfacial interaction parameter in the "inclusion–matrix" system (p = 1, 0.5, and 0 for coherent, semicoherent, and incoherent interfaces,[1] respectively); and $q = E_m/E_i$, ratio of cohesion energies of the matrix to inclusion materials. Expression (10) is qualitatively consistent with the data reported in [46, 47]: The melting temperature of nanoobjects coherent with the high-melting matrices should exceed that of incoherent nanoobjects {the calculated and experimental decreases in T_m for lead nanowires in the Pb–Al (matrix) system [48] reasonably agree}.

The increase in T_m in terms of the Debye theory was also assessed by Rekhviashvili et al. [49] via analyzing the change in the amplitude of root-mean-square fluctuations of atoms on the surface and in the bulk of nanoparticles. In that study, it was suggested that Tolman's equation relating the surface energy to the pore radius be transformed into $\sigma(r) = \sigma/(1 + 2\xi/r)$, where ξ is the Tolman's constant. For details on melting and superheating phenomena in macro- and nanocrystals, see [47].

Gromov et al. [39, 50] examined the behavior of copper, iron, and nickel films on inert SiO_2 and Al_2O_3 substrates and attempted elucidating how T_m varies with the film thickness, considering the changes in the enthalpy of melting, surface energy, and condition of the interface during melting. The film melting–dispersion processes were studied by measuring the electrical resistance and examining the film surface by scanning electron microscopy. It was shown that decreases in melting temperature for thin films are induced by changes in the surface energy and heat of melting in solid–liquid phase transition, as well as by interface modification associated with dispersion. Film melting originates in local segments and subsequently spreads over the entire film; the process has a temperature-dependent activation nature. For example, the range corresponding to decline in conductivity during melting of a thin (20-nm-thick) copper film at 803 K is five times narrower than that at 743 K [50].

Size-dependent effects have implications for other phase transformations in nanomaterials (Table 1). The

[1] Here, coherent, incoherent, and semicoherent interfaces imply those coherent in lattice periods and other physicomechanical properties, lacking coherence, and representing an intermediate (or mixed) situation, respectively.

temperature of tetragonal to monoclinic phase transition was determined for ZrO_2 stabilized with minor Y_2O_3 additions. Also studied were powders and sintered briquettes with different sizes of nanoparticles (80–200 nm) and nanocrystallites (200–1000 nm) [63]. Using a thermodynamic approach, the critical sizes of nanoparticles d_c and nanocrystals L_c were related to the transformation temperature T:

$$1/d_c = \Delta H_b(1 - T/T_b)/(6\Delta\sigma). \quad (11)$$

$$1/L_c = \Delta H_b(1 - T/T_b)/(6\Delta S) + \Delta U_d/6\Delta S. \quad (12)$$

Here, ΔH_b и T_b are the enthalpy and temperature of transformation for a coarse-crystalline bulk sample; $\Delta\sigma$ and ΔS, differences between the surface and boundary energies of tetragonal and monoclinic modifications, respectively; and ΔU_d, deformation energy involved in transformation [51, 63].

Extrapolation of the data from [63] to room temperature gave the following critical d and L values, nm, for different compositions:

	ZrO_2	$ZrO_2 + 0.5\%Y_2O_3$	$ZrO_2 + 1.0\%Y_2O_3$	$ZrO_2 + 1.5\%Y_2O_3$
particles (d_c)	15	30	51	71
sintered briquettes (L_c)	–	70	100	155

In yttria-doped zirconia the tetragonal modification exists under smaller than indicated characteristic dimensions. Higher L_c values are associated with the differences in surface and boundary energies, as well as with the contribution made by deformation energy.

The crystallite size also affects the martensite transformation in Fe–Ni and Ti–Ni–Co alloys via decreasing its onset temperature and suppressing these transitions during cooling at certain critical sizes L [64]. If the crystallite size exceeds the critical value, the martensite transition follows the go-ahead mechanism. At the same time, at $L \approx L_c$ the transition "is locked out," and at $L < L_c$ there is no transformation at all, because the nucleus is larger than the crystallite. The volume fraction of martensite M varies with the crystallite size as

$$M = M_o - K_m L^{-0.5}, \quad (13)$$

where M_0 и K_m are constants.

Nonequilibrium phases have long been observed in thin films. As early as more than half a century ago, Bublik and Pines [65] employed a thermodynamic approach to derive the precondition to phase transition associated with changes in thin film thicknesses. At smaller than critical (h_0) thicknesses, films can comprise unusual phases because of the contribution made by excess free energy. The parameter h_0 is determined by the expression:

$$h_0 = (\sigma_1 - \sigma_2)/(F_2 - F_1), \quad (14)$$

where indices 1 and 2 refer to the equilibrium and nonequilibrium phases, respectively, and σ_i and F_i are the surface and free energies of these phases, respectively.

Calculation by formula (14) gives a quite plausible result, $h_0 \approx 10$ nm. The concept advanced in [65] was implemented in numerous studies to determine the critical size of nanoobjects. However, those studies employed a different approach to analyze how the total free energy (i.e., that incorporating the surface contribution) affects the nanoparticle size(thin film thickness) $r(h)$. For example, Morokhov et al. [66] performed more detailed calculations of some characteristic features of the phase diagrams for ultradispersed systems. Unfortunately, the approaches advanced in [65, 66] are nearly forgotten now and not cited by modern Russian, and especially foreign researchers.

Further impetus to phase composition studies for thin objects came from extensive application of multilayered films, the so-called superlattices comprising hundreds of layers with a total thickness of about several micrometers [Ti–Al (Nb, Zr), TiN–AlN (NbN), Fe–Cr, and other systems]. Calculations predicted triphasic fields for multilayered Zr/Nb films (Fig. 2) [67]. The integrated calculations of the free energy took into account both the differences in the interfacial surface energy of metastable and stable components and the deformation energy associated with the features of elastic properties and dislocation structure of the components. The calculated and experimental (X-ray diffraction and microdiffraction) data reasonably agree. The equilibrium phases (hcp-Zr and bcc-Nb) were observed only in region # 1 (see Fig. 2) with the total film thickness $\lambda_\Sigma = h_{Nb} + h_{Zr}$ varying nonmonotonically with the niobium content. At Nb concentrations under 30 vol % and small λ_S values there exists a nonequilibrium hcp–Nb phase (region #3), and at Nb content above 30 vol %, a nonequilibrium bcc–Zr phase (region # 2).

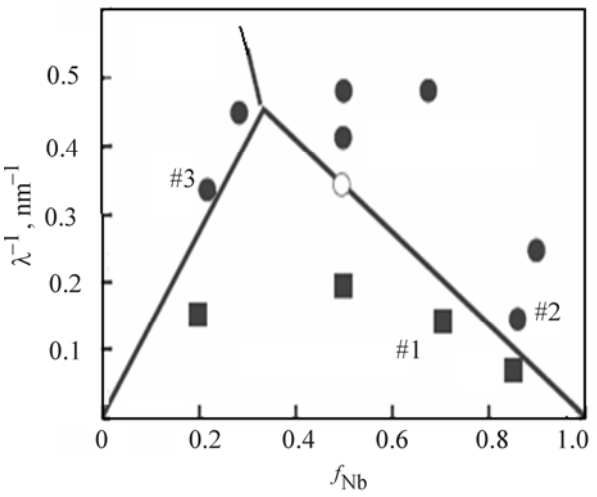

Fig. 2. Phase diagram of multilayered Zr/Nb films [67]. The diagram is constructed in coordinates of the volume fraction of niobium f_{Nb} vs. superlattice parameter (the sum of the thicknesses of individual layers $\lambda_\Sigma = h_{Nb} + h_{Zr}$). (Points) Experimental and (lines) calculated data. (#1) The hcp-Zr)/bcc-Nb, (#2) bcc-Zr/bcc-Nb, and (#3) hcp-Zr/hcp-Nb stability regions.

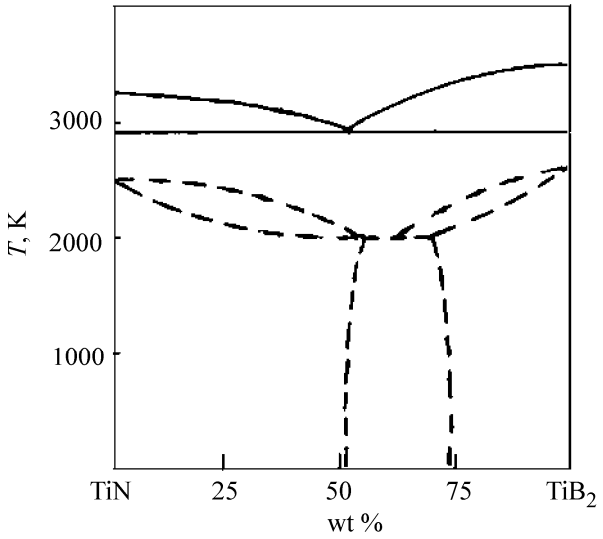

Fig. 3. Phase diagram of (solid lines) coarse-crystalline and (dashed line) filmed TiB_2–TiN samples (grain size ~10 nm)

Phase diagrams (entire or as individual segments) adjusted to size-dependent effects were calculated, e.g., for ZrO_2–Y_2O_3 [51], Pb–Bi [68], carbon [69–71], TiB_2–TiN [72], TiB_2–B_4C [73], and metal–hydrogen [74]). Figure 3 presents the pseudobinary phase diagram for a coarse-crystalline TiB_2–TiN sample characterized by a very poor mutual solubility of the components at room temperature. The dashed line represents the diagram for nanostructured films, in which, according to X-ray phase analysis data, the mutual solubility of the components is basically different. The decrease in the eutectic temperature for the films was estimated in the regular solution approximation, with the free energy of the solid phase incorporating the contribution from excess surface energy, associated with nanocrystallinity [75]. The calculations employed an approximate theory, and there were no data on the surface energy at nanograin boundaries. Combined, these factors resulted in deriving no more than estimated values. In [73] the surface energy of 1–3 J m^{-2} was taken for TiB_2–B_4C nanostructured films (L = 5–10 nm).

Solid solutions of hydrogen in nanocrystalline metal (Pd) and intermetallic (TiFe, $LaNi_5$) [74] samples exhibited a substantial increase in solubility and narrowing of biphasic fields. The latter disappear upon changing from nanocrystals to amorphous objects. Weissmüller and Lemier [76] employed solid mechanics equations for elucidating how the stress in interstitial solid solutions affects the critical temperature of phase decomposition in Pd–H_2 nanocrystalline alloys. As shown theoretically and experimentally for nanocarbon [69–71], a decrease in the particle size is accompanied by shifting of the graphite–diamond–liquid equilibrium to lower temperatures and higher pressures in the phase diagram.

For various aspects of solubility of nanoalloy components and evolution of phase diagrams, see also [77–79].

One way to improve the mechanical properties of nanomaterials and their thermal stability lies in spinodal decomposition of solid solutions, yielding a stable biphasic nanostructure. Theoretical studies of how the solid solution decomposition kinetics is affected by grain boundaries [80] showed the following. In the case of boundary segregations, the degree of decomposition tends to increase with grain size decreasing to the critical size. Of special interest is the pseudobinary system TiN–AlN incorporating metal-like titanium nitride (cubic NaCl type structure) and covalent aluminum nitride (hexagonal ZnS–type wurtzite structure). Decomposition of the single-phase solid solution $(Ti_{1-x}Al_x)N$ with the cubic structure ($x \leq$

Table 2. Superconducting and electronic heat properties of $Cu_{90}Nb_{10}$ composite and bulk copper and niobium samples [82]

Sample	Electronic heat capacity, mJ mol^{-1} K^{-1}	Curie temperature T_C, K	Debye temperature Θ, K
$Cu_{90}Nb_{10}$, initial sample, Nb crystallite size ~20 nm	1.20	3–7	328
$Cu_{90}Nb_{10}$, annealed at 477°C, Nb crystallite size ~30 nm	1.68	7.0	348
$Cu_{90}Nb_{10}$, coarse-grained, annealed at 770°C	1.40	8.8	319
Nb, in nanocomposite	3.00	3–7	240
Nb, bulk sample	8.50	9.2	252
Cu, bulk sample	0.73	–	334

0.7) is observed at ~973 K. This is accompanied by an increase in hardness, beneficial in terms of preparation of thermally stable tool materials. Mayrhofer et al. [81] found that the spinodal decomposition kinetics for that system was affected by varied contributions from the surface and deformation energies. In this context, a highly indicative study could be found in examination (still to be undertaken) of the temperature and kinetic features of spinodal decomposition as influenced by thin film thickness.

Phonon Spectrum, Electronic Heat Capacity, Superconducting Transition Temperature, and Conductivity Type

Zemlyanov et al. [82, 83] examined the size-dependent behavior of phonon spectrum and size-dependent effects in electronic and superconducting properties of Cu–Nb and Cu–Pb nanocomposites prepared by quenching from liquid state. As shown by inelastic neutron scattering examinations, the density of low-energy vibrations of atoms in $Cu_{90}Nb_{10}$ nanocomposite exceeds that in coarse-crystalline sample. Hence, nanostructured state is characterized by low-energy modes associated with changes in vibrations of atoms with increasing interface proportion. Table 2 lists the measured electronic heat capacity γ, superconducting transition temperature T_C, and Debye temperature Θ for $Cu_{90}Nb_{10}$ composite against those for bulk copper and niobium samples. Niobium and lead nanoinclusions in $Cu_{90}Nb_{10}$ composite (as well as in $Cu_{85}Pb_{15}$ and $Cu_{50}Pb_{50}$) lead to smearing of the super-conducting transition and decreases in T_C, Θ, and γ. A change in the electronic heat capacity implies a decrease in the electronic density of states at the Fermi level in the nanocrystalline structure.

Size-dependent effects in superconducting properties of Pb, Nb, MgB_2, Bi, and Al nanoobjects were also examined by other researchers (see, e.g., [84–87]). The theoretically calculated increase in T_C with decreasing nanostructure size [84] was validated experimentally for Al nanoparticles and thin films only [85]. For other objects T_C tends to decrease with decreasing crystallite size.

Calculations for niobium films (0.5-μm-thick) by Bose et al. [87] revealed a monotonic decrease with decreasing crystallite size for T_C and ratio of electrical resistivities at 300 and 10 K ρ(300 K)/ρ(10 K), as well as a nonmonotonic increase for the upper critical field $H(C_2)$. This pattern for H_{C2} was associated with two competing opposite factors, decreased density of states at the Fermi level and progressive carrier scattering at grain boundaries with decreasing crystallite size [decrease in the ρ(300 K)/ρ(10 K) ratio]. Increase in $H(C_2)$ for nanomaterials was also observed for other type II superconductors (nitrides, carbides, etc.) [88].

Of much interest are the data on the grain and nanotwinned interlayer boundaries, reported by Shen et al. [89]. Specifically, the nanotwinned interlayer boundaries in copper affect the mechanical properties in a manner similar to that characteristic for grain boundaries in nanometals. At the same time, the nanotwin boundaries are transparent for conduction carriers (electrons). By contrast to conventional nanocrystalline objects, such nanoobjects are characterized by high strength and plasticity, and their electrical conductivity is identical to that of poorly stable coarse-crystalline copper.

The revealed phenomenon offers a scope for preparation of high-strength plastic copper with high

conductivity, suitable for manufacturing super-abrasion-resistant contacts for electrotechnical applications.

By contrast to metals and alloys, a series of oxides (TiO_2, ZrO_2 + 10%Y_2O_3, CeO_{2-x}) undergo substantial conductivity alterations in changing from coarse-crystalline to nanocrystalline objects [90–92]. Specifically, the electrical conductivity increases and the conduction activation energy decreases, which observations were explained by the specific features of conduction at interfaces. Relevant calculations showed that the conductivity along the interface, as controlled by grain boundary diffusion, exceeds by several orders of magnitude the conductivity of single crystals and thick films, controlled by bulk diffusion only [91]. The conduction activation energy Q decreases by more than half, from 1.04 to 0.45 eV (for a 15-nm-thick film Q was experimentally estimated at 0.62 eV).

Importantly, Chiang et al. [93] revealed an opposite effect for ZrO_2 + 3%Y_2O_3 samples. Specifically, on changing from coarse-crystalline to nanocrystalline objects the conductivity decreased by approximately two orders of magnitude, and the activation energy, increased. This is evidently due to the specific structure of boundaries (this phenomenon deserves special study).

Klinchuk et al. [94] expressed the decrease in the conduction activation energy Q for nanostructured oxides as follows:

$$Q = Q_0 - (4\lambda v/L)\ \mathrm{cth}\ (4\lambda v/LkT), \qquad (15)$$

where Q_0 is the conduction activation energy in a single crystal, and v, volume of oxygen vacancy.

In deriving formula (15) it was presumed that diffusion of oxygen vacancies is affected by significant Laplace pressure associated with essential curvature of the nanograin surface. The calculated and experimental results reasonably agree. The major contribution to conductivity increase in nanostructured ZrO_2 + 16% Y_2O_3 samples comes from interfaces.

Intensification of researches into nanowires increased the interest in their electrical properties (see, e.g., [95–97]). The measured temperature dependence of the electrical resistance suggests semiconductor behavior of bismuth nanowires [95]. The size-dependent effects are evident from the following data:

Rectangular cross-section width, nm	70	120	200
Electrical resistance at 300 K, mΩ cm	4.05	2.87	2.30

The mean free path for electrons in bismuth lattice is close to 100 nm. As shown by Chiu and Shih [95], the charge carrier scattering at grain boundaries is primarily responsible for the observed increase in electrical resistance, caused by decrease in nanowire cross section, while scattering on the nanowire surface is of minor importance.

With crystallite size decreasing because of phonon scattering at intercrystallite boundaries, the thermal conductivity of nanomaterials tends to decrease. This was demonstrated, e.g., for diamond films and yttrium-stabilized zirconia. For the latter object, the thermal conductivity decreased 2–2.5 times with crystallite size decreasing from 100 to 10 nm [13, 98].

The possibility to control the thermal and electrical conductivities via nanostructuring is of much practical significance. Specifically, this opens prospects for developing efficient thermoelectric materials characterized by a high figure of merit $Z = (a^2\lambda)/\chi$ (a is thermal emf; λ, electrical conductivity; and χ, thermal conductivity). An increase in the figure of merit on changing to nanomaterials is associated with the fact that a decrease (or minor change) in the numerator ($a^2\lambda$) of the above-given expression is compensated by a decrease in χ. Chen et al. [99] examined PbTe/PbSeTe- and Bi_2Te_3/Sb_2Te_3-based multilayered compositions (superlattices) and revealed a 2–5-fold increase in the figure of merit, caused by a decrease in thermal conductivity in changing from conventional coarse-crystalline samples to nanostructures.

Studies of the galvanomagnetic and electrical characteristics of nanostructured TiN films as influenced by the crystallite size [100] showed the following. Nearly threefold grain size reduction leads to a significant (nearly tenfold) decrease in conductivity without affecting the Hall coefficient. Hence, the concentrations of carriers (primarily, electrons) in films with different crystallite sizes are virtually identical, and the difference in the carrier mobilities is associated with scattering on crystallite boundaries.

There are significant amounts of oxygen and carbon impurities in the films examined. In this situation, their boundary segregations, TiO and TiC, could be formed, for which the carrier concentration considerably differs from that for TiN. The revealed identical carrier concentrations in these films suggest a nearly uniform distribution of oxygen and carbon in the bulk and on the boundaries of crystallites throughout the examined range of crystallite sizes.

CONCLUSIONS

The above discussion by no means covers the entire spectrum of the latest data pertinent to size-dependent and interface effects in physicochemical properties of consolidated nanomaterials. Further studies are needed to identify the "pure" role of size-dependent effects, since the true contribution from various factors to nanomaterial properties often remains "off-screen." Of much significance will be elucidation of the nature of interfaces (grain and phase boundaries) which can be of fundamental importance for the melting temperature and conductivity of nanomaterials, in which situation size-dependent effects have ambiguous implications. Interface effects are specifically responsible for difficulties in analyzing the applicability for nanoscale of the classical relationships describing the size dependence of the properties of disperse systems [Laplace, Thomson (Kelvin), Gibbs-Ostwald, and other formulas].

We stated from the outset that size-dependent effects in mechanical, catalytic, and biological properties of nanoobjects, as well as the cluster aspects, are beyond the scope of this study.[2] The same is true of nanopolymer, nanocarbon, and nanobiological (and especially hybrid) materials characterized by a complex organizational hierarchy. To our knowledge, size-dependent effects in those nanomaterials have received little research efforts so far [104], except for studies of glass transition points of polymer threads and films [13, 20].

It should also be noted that, here, we considered size-dependent effects in fairly simple stereologic nanoobjects (nearly equiaxed and uniform in size nanocrystallites and single- and multilayered films). Pokropivny and Skorokhod [106] suggested that the number of types of nanostructures comprised of nanocrystallites with different shapes and compositions be increased from 12 (as proposed in Gleiter's classification [105]) to 36, so as nanotubes and other building blocks be also included. Account should be made not only of the average size of grains (phase inclusions, pores) or tube diameter (film thickness) but also of the size distribution of these parameters. To this end, appropriate size distribution functions should be introduced. Further complications come from the fractal nature of some nanoobjects (e.g., film surface [107]) or bimodal grain size distribution [108, 109].

Thus, stereologic characteristic of the structure types of nanomaterials is required for better understanding of the role played by size-dependent effects and interfaces in their properties.

Lastly, many classical parameters relevant to transport phenomena (thermal and electrical conductivity, diffusion, and viscosity coefficients), as well as to thermodynamics of reversible and irreversible processes ("phase," "solution," "activity," "surface energy," "interchange coefficients," etc.) are not unconditionally applicable to the entire nanometer range (i.e., down to ~1 nm). Thus, more extensive theoretical and experimental researches on this subject are urgently needed.

[2] For analysis of the strength and plasticity of metallic, ceramic, and carbon nanomaterials, as well as of their catalytic characteristics, see [101–103].

ACKNOWLEDGMENTS

This study was financially supported by the Basic Research Program of the Presidium of the Russian Academy of Sciences (P-8 and P-27 subprograms) and Russian Foundation for Basic Research (project nos. 08-03-00105 and 07-03-11004).

REFERENCES

1. Andrievskii, R.A. and Glezer, A.M., *Fiz. Met. Metalloved.*, 1999, vol. 88, no. 1, pp. 50–73.
2. Andrievskii, R.A. and Glezer, A.M., *Fiz. Met. Metalloved.*, 2000, vol. 89, no. 1, pp. 91–112.
3. Roldugin, V.I., *Usp. Khim.*, 2000, vol. 69, no. 10, pp. 889–922.
4. Summ, B.D. and Ivanova, N.I., *Usp. Khim.*, 2000, vol. 69, no. 11, pp. 995–1008.
5. Uvarov, N.F. and Boldyrev, V.V., *Usp. Khim.*, 2001, vol. 70, no. 4, pp. 307–329.
6. Petrii, O.A. and Tsirlina, G.A., *Usp. Khim.*, 2001, vol. 70, no. 4, pp. 330–344.
7. Andrievski, R.A. and Glezer, A.M., *Scr. Mater.*, 2001, vol. 44, p. 1621–1625.
8. Weissmüller, J., in *Nanocrystalline Metals and Oxides: Selected Properties and Applications*, Knauth, P. and Schonman, J., Eds., Boston: Kluwer, 2001, pp. 1–39.
9. Weissmüller J., in Proc. *22nd Riso Int. Symp. on Materials Science: Science of Metastable and Nanocrystalline Alloys Structure, Properties and Modelling*, Dinesen, A.R., Eldrup, M., Jensen, D.J., Linderoth, S., Pederson, T.B., Pryds, N.H., Pedersen, A., and Wert, J A., Eds., Roskilde (Denmark): Riso National Laboratory, 2001, pp. 155–175.

10. Buler, P., *Nanotermodinamika*, St. Petersburg: Yanus, 2004.
11. Poole, C.P., Jr. and Owens, F.J., *Introduction to Nanotechnology*, New York: Wiley, 2003.
12. Stroyuk, A.L., Kryukov, A.I., Kuchmii, S.Ya., and Pokhodenko, V.D., *Teor. Eksp. Khim*., 2005, vol. 41, no. 2, pp. 67–85.
13. Andrievskii, R.A. and Ragulya, A.V., *Nanostrukturnye materialy* (Nanostructured Materials), Moscow: Izd. Tsentr "Akademiya," 2005.
14. Gusev, A.I., *Nanomaterialy, nanostruktury, nanotechnologii* (Nanomaterials, Nanostructures, Nanotechnologies), Moscow: FIZMATLIT, 2005.
15. Andrievskii, R.A., *Nanostrukt. Materialoved*., 2005, no. 1, pp. 5–13.
16. Rusanov, A.I., *Surf. Sci. Rep*., 2005, vol. 58, pp. 111–239.
17. Suzdalev, I.P., *Nanotekhnologiya: fiziko-khimiya nanoklasterov, nanostruktur i nanomaterialov* (Nanotechnology: Physical Chemistry of Nanoclusters, Nanostructures, and Nanomaterials), Moscow: KomKniga, 2006.
18. Rusanov, A.I., *Kolloid. Zh*., 2006, vol. 68, pp. 368–374.
19. Sergeev, G.B., *Nanokhimiya* (Nanochemistry), Moscow: Knizhnyi Dom "Universitet," 2006.
20. Roduner, E., *Nanoscopic Materials: Size-Dependent Phenomena*, Cambridge: RSC Publishing, 2006.
21. *Nanomaterials and Nanochemistry*, Bréchignac, C., Houdy, P., and Lahmani, M., Eds., Berlin: Springer, 2007.
22. Andrievskii, R.A., *Ross. Khim. Zh. (Zh. Ross. Khim. O–va im. D. I. Mendeleeva)*, 2002, vol. 46, no. 5, pp. 50–56.
23. Bazulev, A.N., Samsonov, V.M., and Sdobnyakov, N.Yu., *Zh. Fiz. Khim*., 2002, vol. 76, no. 11, pp. 2073–2076.
24. Samsonov, V.M., *Izv. Ross. Akad. Nauk, Ser. Fiz*., 2005, vol. 69, pp. 1036–1038.
25. Magomedov, M.N., *Fiz. Tverd. Tela*, 2004, vol. 46, no. 5, pp. 924–936.
26. Magomedov, M.N., *Zh. Fiz. Khim*., 2005, vol. 79, no. 5, pp. 829–835.
27. Ouyang, G., Tan, X., and Yang, G., *Phys. Rev. B*, 2006, vol. 74, p. 195408.
28. Lu, H.M. and Jiang, Q., *Langmuir*, 2005, vol. 21, pp. 779–786.
29. Nanda, K.K., *Appl. Phys. Lett*., 2005, vol. 87, p. 021909.
30. Vanithakumari, S.V. and Nanda, K.K., *J. Phys. Chem. B*, 2006, vol. 110, pp. 1033–1039.
31. Nanda, K.K., Kruis, F.E., and Fissan, H., *Phys. Rev. Lett*., 2002, vol. 89, p. 256103.
32. Nanda, K.K., Maisels, A., Kruis, F.E., Fissan, H., and Stappert, S., *Phys. Rev. Lett*., 2003, vol. 91, p. 106102.
33. Schroeder, A., Fleig, J., Drings, H., et al., *Solid State Ionics*, 2004, vol. 173, pp. 95–99.
34. Caro, A. and Van Swygenhoven, H., *Phys. Rev. B*, 2001, vol. 63, pp. 134101 (1–8).
35. Lu, K. and Sun, N.X., *Phil. Mag. Lett*., 1997, vol. 75, pp. 389–393.
36. Ouyang, G., Liang, L.H., Wang, C.X., et al., *Appl. Phys. Lett*., 2006, vol. 88, p. 091914.
37. Summ, B.D., *Osnovy kolloidnoi khimii* (Fundamentals of Colloid Chemistry), Moscow: Izd. Tsentr "Akademiya," 2006.
38. Samsonov, V.M., Dronnikov, V.V., and Mal'kov, O.A., *Zh. Fiz. Khim*., 2004, vol. 78, no. 7, pp. 1203–1210.
39. Gromov, D.G., Gavrilov, S.A., Rodichev, E.N., et al., *Zh. Fiz. Khim*., 2006. vol. 80, no. 10, pp. 1856–1862.
40. Xiao, S., Hu, W., and Yang, J., *J. Chem. Phys*., 2006, vol. 125, p. 184504.
41. Guisbiers, G. and Wautelet, M., *Nanotechnology*, 2006, vol. 17, pp. 2008–2012.
42. Rekhviashvili, S.Sh. and Kishtikova, E.V., *Pis'ma Zh. Tekh. Fiz*., 2006, vol. 32, no. 10, pp. 50–58.
43. Qi, W.H., *Physica B*, 2005, vol. 368, pp. 46–53.
44. Zhong, J., Zhang, L.H., Jin, Z.H., et al., *Acta Mater.,* 2001, vol. 49, pp. 2897–2904.
45. Xu, Q., Sharp, I.D., Yuan, C.W., et al., *Phys. Rev. Lett*., 2006, vol. 97, p.155701.
46. Sheng, H.W., Ren, G., Peng, L.M., et al., *Phil. Mag. Lett*., 1996, vol. 73, no. 4, pp. 179–186.
47. Mei, Q.S. and Lu, K., *Progr. Mater. Sci*., 2007, vol. 52, pp. 1175–1196.
48. Qi, W.H., *Mod. Phys. Lett*., 2006, vol. 20, pp. 1943–1946.
49. Rekhviashvili, S.Sh., Kishtikova, E.V., Karmokova, A.M., et al., *Pis'ma Zh. Tekh. Fiz*., 2007, vol. 33, no. 2, pp. 1–8.
50. Gromov, D.G., Gavrilov, S.A., Rodichev, E.I., et al., *Fiz. Tverd. Tela*, 2007, vol. 49, no. 1, pp. 172–178.
51. Suresh, A., Mayo, M.J., and Porter, W.D., *J. Mater. Res*., 2003, vol. 18, pp. 2912–2921.
52. Sato, H., Kitakami, O., Sakurai, T., et al., *J. Appl. Phys*., 1997, vol. 81, pp. 1858–1866.
53. Shi, W., Kong, J., Shen, H., et al., *Vacuum*, 1992, vol. 42, pp. 1070–1074.
54. Asaka, K., Hirotsu, Y.Y., and Tadaki, T., *Mater. Sci. Eng. A*, 1999, vols. 272–275, pp. 262–269.
55. Winterer, M., Nitsche, R., Redfern, S.A.T., et al., *Nanostruct. Mater*., 1995, vol. 5, pp. 679–686.
56. Garvie, R.C. and Goss, M.C., *J. Mater. Sci*., 1986, vol. 21, pp. 1253–1263.
57. Chraska, T., King, A.H., and Berndt, C.C., *Mater. Sci. Eng. A*, 2000, vol. 286, pp. 169–176.
58. Ji, Z., Haynes, J.A., Ferber, M.K., et al., *Surf. Coat. Technol*., 2001, vol. 135, pp. 109–116.
59. Akdogan, E.K., Mayo, W., Safari, A., et al., *Ferroelectrics,* 1999, vol. 223, pp. 11–19.

60. McHale, J.M., Auroux, A., Perrotta, A.J., et al., *Science,* 1997, vol. 277, pp. 788–796.
61. Hahn, H., Skandan, G., and Parker, J.C., *Scr. Metal. Mater*., 1991, vol. 25, pp. 2389–2396.
62. Alivisatos, A.P., *Ber. Bunsenges. Phys. Chem.*, 1997, vol. 101, pp. 1573–1578.
63. Suresh, A., Majo, M.J, Porter, W.D., et al., *J. Am. Ceram. Soc*., 2003, vol. 86, p. 360–362.
64. Glezer, A.M., Blinova, E.N., and Pozdnyakov, V.A., *Izv. Ross. Akad. Nauk., Ser. Fiz*., 2002, vol. 66, pp. 1263–1275.
65. Bublik, A.I. and Pines, B.Ya., *Dokl. Akad. Nauk SSSR*, 1952, vol. 87, pp. 215–218.
66. Morokhov, I.D., Trusov, L.I., Kats, E.I., et al., *Dokl. Akad. Nauk SSSR*, 1981, vol. 261, pp. 850–854.
67. Thompson, G.B., Banerjee, R., Dregia, S.A., et al., in *Nanostructured Interfaces*, Plitzko, J.M., Duscher, G., Zhu, Y., and Ichinose, H., Eds., vol. 727, Warrendale: Mat. Res. Soc. Proc., 2002, p. R5.8.
68. Jesser, W.A., Shneck, R.Z., and Gile, W.W., *Phys. Rev. B*, 2004, vol. 69, p. 144121.
69. Huang, F., Tong, Y., and Yun, Sh., *Fiz. Tverd. Tela*, 2004, vol. 46, pp. 601–605.
70. Vereshchagin, A.L., *Fiz. Goren. Vzr*., 2002, vol. 38, pp. 119–124.
71. Danilenko, V.V., *Fiz. Goren. Vzr*., 2005, vol. 41, pp. 110–116.
72. Andrievskii, R.A. and Kalinnikov, G.V., *Fiz. Khim. Stekla*, 2007, vol. 33, no. 4, pp. 483–489.
73. Kalinnikov, G.V., Andrievskii, R.A., Kopylov, V.N., and Louzguine, D., *Fiz. Tverd. Tela*, 2008, vol. 50, no. 2, pp. 359–363.
74. Andrievskii, R.A., *Usp. Fiz. Nauk*, 2007, vol. 177, no. 7, pp. 721–735.
75. Andrievskii, R.A., *Zh. Ross. Khim. O–va. im. D. I. Mendeleeva*, 1991, vol. 36, no. 2, pp. 137–144.
76. Weissmüller, J. and Lemier, C., *Phil. Mag. Lett*., 2000, vol. 80, pp. 411–414.
77. Koshkin, V.M. and Slezov, V.V., *Pis'ma Zh. Tekh. Fiz*.., 2004, vol. 30, no. 9, pp. 38–43.
78. Shirinyan, A.S., Gusak, A.M., and Wautelet, M., *Acta Mater.,* 2005, vol. 53, pp. 5025–5032
79. Weissmüller, J., Bunzel, P., and Wilde, G., *Scr. Mater*., 2001, vol. 51, pp. 813–816.
80. Razumov, I.K., *Cand. Sci. (Phys.-Math.) Dissertation*, Yekaterinburg: Inst. Fiz. Metal. Ural. Otd. Ross. Akad. Nauk, 2005.
81. Mayrhofer, P.H., Fischer, F.D., Bohm, H.J., et al., *Acta Mater*., 2007, vol. 55, pp. 1441–1446.
82. Zemlyanov, M.G., Panova, G.Kh., Syrykh, G.V., and Shikov, A.A., *Fiz. Tverd. Tela*, 2005, vol. 47, no. 2, pp. 350–353.
83. Zemlyanov, M.G., Panova, G.Kh., Syrykh, G.V., and Shikov, A.A., *Fiz. Tverd. Tela*, 2006, vol. 48, no. 1, pp. 128–132.
84. Magomedov, M.N., *Fiz. Tverd. Tela*, 2003, vol. 45, no. 9, pp. 1159–1163.
85. Lang, X.Y. and Jiang, Q., *Sol. State Comm*., 2005, vol. 134, pp. 797–802.
86. Bose, S., Raychaudhuri, P., Banerjee, R., et al., *Phys. Rev. Lett*., 2005, vol. 95, p. 147003.
87. Bose, S., Raychaudhuri, P., Banerjee, R., et al., *Phys. Rev. B*, 2006, vol. 74, p. 224502.
88. Troitskiy, V.N., Domashnev, I.A., Kurkin, E.N., et al., *J. Nanopart. Res.*, 2003, vol. 5, pp. 521–526.
89. Shen, Y.F., Lu, L., Lu, Q.H., et al., *Scr. Mater*., 2005, vol. 52, pp. 989–964.
90. Demetry, C. and Shi, X., *Solid State Ionics*, 1999, vol. 118, pp. 271–279.
91. Guo, X. and Zhang, X., *Acta Mater*., 2003, vol. 51, pp. 2539–2547.
92. Kosacki, I. and Rouleau, Ch.M., Becher, P.B., et al., *Solid State Ionics*, 2005, vol. 176, pp. 1319–1326.
93. Chiang, Y.-M., Lavik, E.B., and Bloom, D.A., *Nanostruct. Mater*., 1997, vol. 9, pp. 633–638.
94. Klinchuk, M.D., Bykov, P.I., and Hilcher, B., *Fiz. Tverd. Tela*, 2006, vol. 48, no. 11, pp. 2079–2084.
95. Chiu, P. and Shih, I., *Nanotechnology*, 2004, vol. 15, pp. 1489–1492.
96. Fedorov, D.V., Zahn, P., and Mertig, L., *Thin Solid Films*, 2005, vol. 473, pp. 346–350.
97. Urban, D.F., Burki, J., Stafford, C.A., et al., *Phys. Rev. B*, 2006, vol. 74, p. 245414.
98. Yang, H.-S., Bai, G.-R., Thompson, L.I., et al., *Acta Mater*., 2002, vol. 50, pp. 2309–2314.
99. Chen, G., Narayanaswamy, A., and Dames, C., *Superlatt. Microstr*., 2004, vol. 35, pp. 161–167.
100. Andrievskii, R.A., Dashevskii, Z.M., and Kalinnikov, G.V., *Pis'ma Zh. Tekh. Fiz*., 2004, vol. 30, no. 22, pp. 1–7.
101. Eletskii, A.V., *Usp. Fiz. Nauk*, 2007, vol. 177, no. 3, pp. 233–274.
102. Andrievskii, R.A. and Glezer, A.M., *Usp. Fiz. Nauk*, 2009, vol. 179, no. 4, pp. 337–358.
103. Parmon, V.N., *Dokl. Ross. Akad. Nauk*, 2007, vol. 413, no. 1, pp. 53–59.
104. Ivanchev, S.S. and Ozerin, A.N., *Vysokomol. Soedin., Ser. B*, 2006, vol. 48, no. 8, pp. 1531–1544.
105. Gleiter, H., *Acta Mater*., 2000, vol. 48, no. 1, pp. 1–29.
106. Pokropivny, V.V. and Skorokhod, V.V., *Mater. Sci. Eng. C*, 2007, vol. 27, pp. 990–994.
107. Serov, I.N., Margolin, V.I., Soltovskaya, I.A., et al., in *Nano- i mikrosistemnaya tekhnika: Ot issledovanii k razrabotkam* (Nano- and Microsystems Techniques: From Research to Development), Mal'tsev, P.P., Ed., Moscow: Tekhnosfera, 2005, pp. 230–241.
108. Ma, E., *JOM*, 2006, vol. 58, no. 4, pp. 49–53.
109. Ievlev, V.M. and Shvedov, E.V., *Fiz. Tverd. Tela*, 2006, vol. 48, no. 1, pp. 133–138.